Analysis of parasitic motion with the constraint embedded Jacobian for a 3-PRS parallel manipulator

Hassen Nigatu, Yun Ho Choi, Doik Kim

▶ **To cite this version:**

Hassen Nigatu, Yun Ho Choi, Doik Kim. Analysis of parasitic motion with the constraint embedded Jacobian for a 3-PRS parallel manipulator. Mechanism and Machine Theory, 2021, 164, pp.104409. ⟨10.1016/j.mechmachtheory.2021.104409⟩. ⟨hal-03265392⟩

HAL Id: hal-03265392

https://hal.science/hal-03265392v1

Submitted on 3 Nov 2023

HAL is a multi-disciplinary open access archive for the deposit and dissemination of scientific research documents, whether they are published or not. The documents may come from teaching and research institutions in France or abroad, or from public or private research centers.

L'archive ouverte pluridisciplinaire **HAL**, est destinée au dépôt et à la diffusion de documents scientifiques de niveau recherche, publiés ou non, émanant des établissements d'enseignement et de recherche français ou étrangers, des laboratoires publics ou privés.

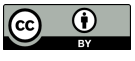

Distributed under a Creative Commons CC BY 4.0 - Attribution - International License

Mechanism and Machine Theory 164 (2021) 104409

Contents lists available at ScienceDirect

Mechanism and Machine Theory

journal homepage: www.elsevier.com/locate/mechmachtheory

Analysis of parasitic motion with the constraint embedded Jacobian for a 3-PRS parallel manipulator

Hassen Nigatu[b,a], Yun Ho Choi[b], Doik Kim[b,*]

[a] Division of Nano & Information Technology, University of Science and Technology (UST), Daejeon 305-350, Korea
[b] Center for intelligent and interactive robotics, Korea Institute of Science and Technology (KIST), Seoul 02791, Korea

ARTICLE INFO

Article history:
Received 14 December 2020
Revised 22 April 2021
Accepted 23 May 2021
Available online 4 June 2021

Keywords:
Parallel manipulator
Kinematics
Constraint
IMS
IRS
Parasitic motion

ABSTRACT

This study derives the equation of parasitic motion of 3-DoFs parallel manipulator from the velocity-level analytic-constraint equation and compares it with a well-known position-level geometric method. The velocity-level constraint is formulated based on the extended Jacobian, derived from the instantaneous motion space (IMS) and the instantaneous restriction space (IRS) for free motion and constraint. In contrast, the position-level constraint, adopted in previous studies, is geometrically obtained by analyzing the moving platform and limb motions. The velocity-level analytic-constraint matrix is used to further analyze the task-space motion. In this paper, the procedure of detecting and identifying the parasitic terms from the independent terms is introduced utilizing the property that comes from the virtue of analytic constraint and inverse rate kinematics algorithm. Then, an equation for the constraint-compatible task motion and a coupling relation between the parasitic and independent motions are derived during further analysis. The paper derived the parasitic motion from position constraint, and an algebraic equivalency with the velocity constraint is shown by taking the time derivative of a point-plane position level constraint for comparison. Finally, numerical simulations are provided to validate the proposed approach and demonstrate the effect of the constraints on the given input velocity within the entire rotational workspace.

© 2021 Elsevier Ltd. All rights reserved.

1. Introduction

Parallel manipulators (PMs) with less than six degrees of Freedom (DoFs) cannot have all motions in $\mathbb{R}^6$ because of the constraints imposed by the limbs that connect the fixed and moving platforms. This type of limited DoFs PM has typically been described using several independent motions equivalent to its DoF. For example, the 3-PRS (prismatic-revolute-spherical) PM has a 3-DoFs motion with three independent motions: translation along the z-axis, and rotation about the x- and y-axes, respectively [1,2]. At this moment, the remaining motions, i.e., translation along the x- and y-axes and rotation about the z-axis, are assumed to have not occurred. However, in reality unexpected motions, known as parasitic motion [1,3,4], occur because of the constraint's nature; these are dependent on the independent 3-DoFs motion.

This unexpected parasitic motion results in inaccurate and undesirable motion of the moving platform; thus, it must be analyzed and eliminated, if possible. Depending on where we deploy the manipulator, the non-zero parasitic motion requires real-time compensation using an extra Cartesian bed [5,6], which leads to complicated control. In addition, it causes

* Corresponding author.
E-mail address: doikkim@kist.re.kr (D. Kim).

https://doi.org/10.1016/j.mechmachtheory.2021.104409
0094-114X/© 2021 Elsevier Ltd. All rights reserved.

difficulty in calibration because the natural controller cannot correct the motion, and thus may it even lead to the damage of the entire system [6]. For instance, the x- and y-axes translational parasitic motion is not required for the 3-PRS manipulator designed for a telescope's tip and tilt motion [7].

To describe the parasitic motion of a 3-PRS PM, a point-plane geometric method has been introduced [1,8–10]. If a point on a rigid body preserves incidence with a known plane, the point is said to be constrained by the plane. Hence, the rigid body motion is guided by the plane, and its constraint equation can be generated from the plane and corresponding normal vector. However, a geometric method cannot be generalized because the geometric constraints obtained differ from mechanism to mechanism except for manipulator having the same constraint. Although the parasitic motion is widely studied [1,6,8,11,12], it is derived from geometric position constraints, and thus, it is critical to accurately identify geometric constraints. Unfortunately, a systematic method for this purpose does not exist. This problem extends the difficulty to the analysis of parasitic motion. In consideration, this paper obtained the parasitic motion entirely from the pure velocity relation and drawn a systematic procedure to distinguish the parasitic terms from the independent task variables.

To describe the PM's velocity, a widely used method for obtaining the system constraints is the reciprocal screw technique. To obtain the reciprocal screw at the velocity level, geometrical [13–18], numerical [19] and analytical [20,21] methods are commonly used. However, to consistently embed, and further analyze the constraints, it is better to use an analytic method. In this study, an analytic velocity-level constraint equation is formulated based on the concept of instantaneous motion space (IMS) and instantaneous restriction space (IRS) of the manipulator [20,22]. With the resulting analytic constraint equation, the parasitic motion analysis is performed directly at the velocity level without considering constraint geometries. To the best of the authors' knowledge, no work examines the parasitic motion directly from the velocity model without considering the geometric position-level constraints.

The IMS and IRS concepts can be briefly described as follows: For PMs, the moving platforms cannot move in the space that cannot be reached by any of the limbs connecting the platform. Thus, PMs with less than six-DoFs also have limbs less than six-DoFs to restrict the moving platform motion [15,23,24]. The output DoFs of these limbs is described by the linear combination of f independent screws associated with each kinematic pair of that particular limb (leg). If $f < 6$, the limb movements can be represented with f motion screws that form a subspace called the IMS. The remaining subspace with $6 - f$ independent screws can be considered as a subspace that cannot be reached by the limbs, and thus represents the subspace for constraints known as the IRS. The IMS of a PM is an intersection of all the IMS of its limbs, i.e., the moving platform can be reached wherein all the limbs can have motions together. On the other hand, the IRS of a PM is a union of all the IRSs of its limbs, i.e., the moving platform cannot be reached whereby any one limb cannot have motions. A complete kinematic description of a PM, particularly with less than 6-DoFs, can be obtained by considering these two sub-spaces simultaneously. The rest of the paper is organized as follows: Section 2 introduces the basic kinematic description of an example manipulator. Section 3 derives a geometric position constraint, and Section 4 formulates the analytic velocity-level constraint based on IMS and IRS of the manipulator. Section 5 discusses the constraint matrix property and compares the position- and velocity-level constraints. Using the null-space projection of constraint matrix, Section 5.1 showed automatic implicit handling of the parasitic motion. Hence, the constraint-compatible velocity is obtained without explicit derivation of parasitic motion equation. Then, the procedure to detect and identify the parasitic terms is presented in Section 5.2. However, considering the importance of analytic coupling relation between parasitic and independent terms of the task-space variables, an explicit parasitic motion equation is obtained solely from velocity constraint in Section 5.3. In Section 6, numerical validation is presented, and the paper is concluded in Section 7.

2. Structural description of 3-PRS manipulator

This section introduces the kinematic architecture and position relation of the 3-PRS parallel manipulator shown in Fig. 1, which is used an example manipulator to analyze constraints and parasitic motion. The mechanism has three identical limbs connecting the two symmetrical plane platforms inscribed in a circle. Frames $\{O_f\}$ and $\{O_m\}$ are the fixed and moving coordinates attached to the center of the corresponding plates, respectively. The radially installed prismatic actuator at the base generates a limb motion along with the revolute and spherical passive joints. The passive spherical joints located at A_i and the revolute joint at B_i connect the moving platform to the fixed platform via a fixed-length link. Vector $\boldsymbol{p}$ is the position of the moving platform in the fixed frame $\{O_f\}$, whereas $\boldsymbol{l}_i$ is a vector along the leg from B_i to A_i. Joint A_i on the moving platform is represented by vector $\boldsymbol{a}_i$ directed from O_m to A_i in the fixed frame, and $\boldsymbol{a}_i = \boldsymbol{R}\boldsymbol{a}'_i$, where $\boldsymbol{R}$ is the rotation matrix of the moving platform and $\boldsymbol{a}'_i$ is the constant vector from O_m to A_i in the moving frame $\{O_m\}$. Note that vectors with a prime symbol $(\cdot')$ throughout this paper are constant vectors in their local frame. Angle ξ_i indicates the actuation direction from the x-axis in the horizontal plane. The radius of fixed and moving platforms are denoted by b_i and r_p, respectively.

The varying length vector $\boldsymbol{b}_i$ at the fixed platforms directed from O_f to B_i represents the active prismatic joint. The manipulator is originally presented in [1] to get the optimal parasitic motion at the position level.

2.1. Inverse kinematics

The inverse kinematics (IK) can be obtained using the position closure from Eqs. (1) and (2). For brevity, the position of the spherical joint, $\boldsymbol{r}_i$, for $i = 1, 2, 3$, can be represented with two identical vectors, i.e., a vector along the limbs from the

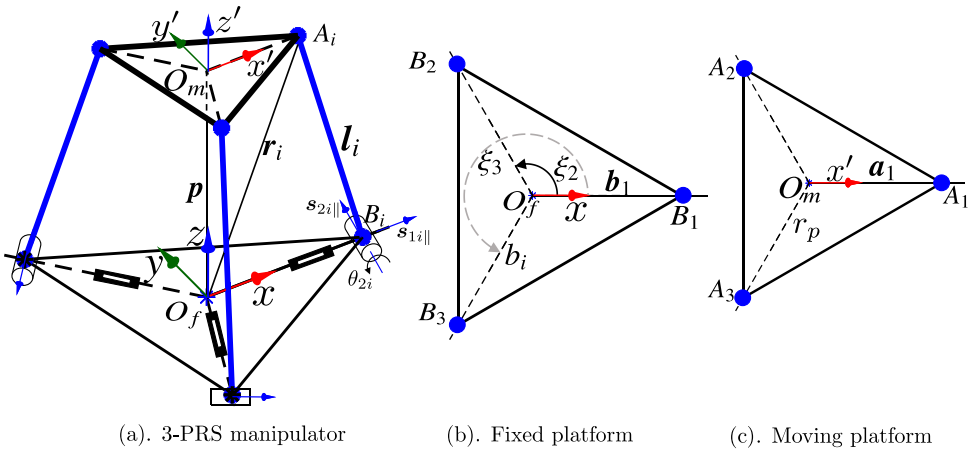

Fig. 1. 3-PRS parallel manipulator kinematic architecture.

fixed plate, Eq. (1) and a vector described with the pose of the moving platform, Eq. (2),

$$\boldsymbol{r}_i = \boldsymbol{R}_z(\xi_i)\boldsymbol{b}_i' + \boldsymbol{R}_z(\xi_i)\boldsymbol{R}_y(\theta_{2i})\boldsymbol{l}_i' \tag{1}$$

$$= \boldsymbol{p} + \boldsymbol{R}\boldsymbol{a}_i' \tag{2}$$

where $\boldsymbol{b}_i' = \begin{bmatrix} b_i & 0 & 0 \end{bmatrix}^T$, $\boldsymbol{l}_i' = \begin{bmatrix} 0 & 0 & l \end{bmatrix}^T$. Vector $\boldsymbol{a}_i'$ is the position of spherical joints based on the moving platform that can be mathematically described as:

$$\boldsymbol{a}_i' = \boldsymbol{R}_z(\xi_i)\boldsymbol{r}_p \tag{3}$$

where $\boldsymbol{r}_p = \begin{bmatrix} r_p & 0 & 0 \end{bmatrix}^T$. Position of the moving platform based on the fixed frame is represented by vector $\boldsymbol{p} = \begin{bmatrix} x & y & z \end{bmatrix}^T$. The rotation matrix of the moving platform is represented as follows:

$$\boldsymbol{R} = \boldsymbol{R}_z(\phi)\boldsymbol{R}_x(\psi)\boldsymbol{R}_y(\theta). \tag{4}$$

Note that the order of rotation is different from usual Euler or roll-pitch-yaw [1].

Angle $\xi_i = (i-1)\frac{2\pi}{3}$ represents the actuation direction of each leg from the positive x-axis. The position vector $\boldsymbol{r}_i$ is known because the pose, $\boldsymbol{p}$ and $\boldsymbol{R}$, in Eq. (2) are given IK.

Thus, the position closure equation becomes

$$\boldsymbol{R}_z(\xi_i)^{-1}\boldsymbol{r}_i - \boldsymbol{b}_i = R_y(\theta_{2i})\boldsymbol{l}_i'. \tag{5}$$

Let $\boldsymbol{R}_z(\xi_i)^{-1}\boldsymbol{r}_i = \boldsymbol{g}$ and eliminating θ_{2i} from Eq. (5) gives the length of prismatic joint b_i as follows:

$$b_i = g_x \pm \sqrt{l^2 - g_z^2} \tag{6}$$

where the passive revolute joint angle is given by

$$c_{\theta_{2i}} = (g_x - b_i)/l \tag{7}$$

$$s_{\theta_{2i}} = g_z/l. \tag{8}$$

In this paper, note that c and s followed by angular variables represents cosine and sine, respectively.

3. Position level constraint

The manipulator considered in this study has limited DoF because of structural constraints, and thus to analyze the manipulator with constraint-compatible relations, the governing equation of constraints must be obtained. Structural constraints of parallel manipulators with less than 6-DoFs at the position-level is analyzed mainly based on the geometric approach [1,6,10]. Especially, Carretero, *et al.* used a fundamental geometric relations based on the graphical method to define the limb constraint, as shown in Fig. 2.

The process involves identifying the plane that comprises the spherical joint centers A_i, and passes through the revolute joint B_i along the direction vector of the prismatic joint and perpendicular to the direction vector of the revolute joint [1].

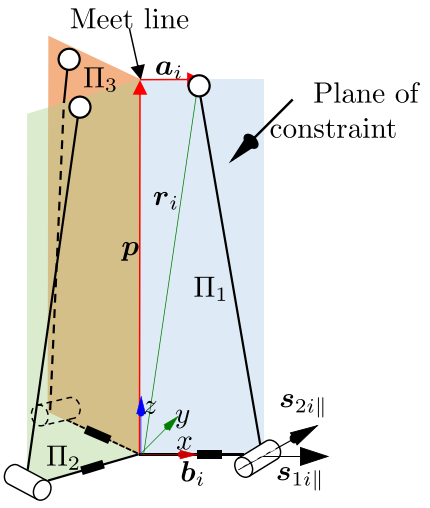

Fig. 2. Kinematic architecture of 3-PRS mechanism.

This means that the distal end of the limb (A_i) is restricted in the plane, and the following algebraic relation can be drawn:

$$\boldsymbol{r}_i^T \boldsymbol{s}_{2i\|} = (\boldsymbol{p} + \boldsymbol{R}\boldsymbol{a}_i')^T \boldsymbol{s}_{2i\|} = \boldsymbol{0}. \tag{9}$$

The direction vector of rotation joint is $\boldsymbol{s}_{2i_\|} = \begin{bmatrix} -s_{\xi_i} & c_{\xi_i} & 0 \end{bmatrix}^T$ and $\boldsymbol{a}_i' = \begin{bmatrix} r_p c_{\xi_i} & r_p s_{\xi_i} & 0 \end{bmatrix}^T$ where $i = 1, 2,$ and 3 for the respective legs.

By substituting elements of the direction vector $\boldsymbol{s}_{2i\|}$ into the left-hand side of Eq. (9), the following relations can be obtained :

$$\begin{aligned} r_{1y} &= 0 \\ r_{2y} &= r_{2x}\tan_{\xi_2} \\ r_{3y} &= r_{3x}\tan_{\xi_3}. \end{aligned} \tag{10}$$

By equating position of the spherical joint and pose of the moving platform, $\boldsymbol{r} = \boldsymbol{p} + \boldsymbol{R}\boldsymbol{a}_i'$ as in Eq. (9) with relations of Eq. (10), the constraints are as follows:

$$y + R_{21} r_p = 0 \tag{11}$$

$$y + R_{21} r_p c_{\xi_2} + R_{22} r_p s_{\xi_2} = \tan_{\xi_2} \left(x + R_{11} r_p c_{\xi_2} + R_{12} r_p s_{\xi_2} \right) \tag{12}$$

$$y + R_{21} r_p c_{\xi_3} + R_{22} r_p s_{\xi_3} = \tan_{\xi_3} \left(x + R_{11} r_p c_{\xi_3} + R_{12} r_p s_{\xi_3} \right). \tag{13}$$

Then, the constrained variable y can be easily obtained from Eq. (11). By summing Eqs. (12) and (13), and substituting y into the resulting equation with rotational elements from Eq. (4), the rotational dependent variable can be obtained:

$$\tan_\phi = \frac{s_\psi s_\theta}{c_\psi - c_\theta}. \tag{14}$$

The remaining dependent variable x can be derived by subtracting Eq. (13) from Eq. (12):

$$x = \frac{1}{2} r_p \left(-c_\phi c_\psi + c_\phi c_\theta + s_\phi s_\psi s_\theta \right) \tag{15}$$

$$y = -r_p c_\psi s_\phi. \tag{16}$$

Since the manipulator in Fig. 1 has only 3-DoFs, the position-level constraint in Eq. (9) is used to describe the inter-relation of dependent and independent task variables as in Eqs. (14), (15) and (16). Thus, θ, ψ and z can be freely chosen whereas x, y and ϕ are dependent on these free variables.

Although the method presented in this section can incorporate constraint information into the motion equation and enables us to describe the position-level coupling relation of task variables, it has the following limitations.

- The point-plane constraint modeling based on the geometric approach is heavily dependent on the structure of a manipulator. It cannot be consistently applied to other manipulators because the geometric approach generally uses different relations from manipulator to manipulator, considering the exception case for manipulators having identical limb constraint.
- It also does not provide any procedural reasoning to distinguish the parasitic (dependent) variables from the main(independent) variables. Designers must use an independent technique or prior knowledge on the manipulator structure.

To overcome these limitations, an analytic formulation of constraints is preferable to analyze the parasitic motion.

4. Velocity level constraint

In Section 2, a 1T2R manipulator with less than 6-DoFs was introduced. For this type of manipulators, the region that cannot be reached by the moving platform because of structural constraints must be taken into account in the design procedure for the accurate understanding of kinematics characteristics in consistent manner. Although several methods have been suggested to embed structural constraints at the velocity level, [16,17,19], an analytic approach outlined by Kim and Chung [20] is adopted to overcome the drawbacks discussed in Section 2.1. In the study, IMS and IRS are introduced to describe the moving platform's motion and constraint.

4.1. Instantaneous motion and restriction space

A general manipulator has instantaneous motion $\dot{\boldsymbol{x}} \in \mathbb{R}^6$, but when subjected to certain constraints, some regions can/cannot be reached by the manipulator, and consequently, said regions need to be taken into account simultaneously. These two regions described with two complementary sub-spaces,IMS and IRS, are defined as :

Instantaneous Motion Space(IMS): is the tangent space of SE(3) spanned by the linearly independent motion vectors at the moving-plate (IMS $\subset \mathbb{R}^6$). From the leg point of view, this space is spanned by the intersection of twists in all legs, and it can be physically interpreted as follows: the motion of the moving platform occurs in the region where all legs commonly work.

Instantaneous restriction Space(IRS): is an orthogonal complementary subspace of the instantaneous motion space in $\mathbb{R}^6$ which belongs to the unreachable region due to the structural constraints and formed by the union of all restriction screws induced from each leg.

PMs' constraints are a union of those legs restriction, and thus the entire motion is described by the legs IMS and IRS in general. In a serial manipulator, IMS ($\mathcal{C}(\boldsymbol{J}_j)$) is obtained from the forward rate kinematics whereas IRS ($\mathcal{C}(\boldsymbol{J}_c)$) is obtained by taking the orthogonal complement ($\mathcal{N}(\boldsymbol{J}_j^T)$). Hence, the IMS fully describes the serial manipulator's motion, and the corresponding IRS is {6 - IMS} which represents the space that the manipulator cannot reach. Thus, the generic extended forward-rate kinematics (FRK) of an isolated limb can be written with the (6×6) extended Jacobian $\boldsymbol{J}_e$ as follows:

$$\dot{\boldsymbol{x}} = \boldsymbol{J}_e \dot{\boldsymbol{q}}_e = \begin{bmatrix} \boldsymbol{J}_j & ; & \boldsymbol{J}_c \end{bmatrix} \begin{bmatrix} \dot{\boldsymbol{q}} \\ \boldsymbol{0} \end{bmatrix} \tag{17}$$

where $\dot{\boldsymbol{x}}$ and $\dot{\boldsymbol{q}}_e$ denote the velocity of the end-effector and extended joint velocity, respectively. The dimension of $\boldsymbol{J}_j$ is a $(6 \times f)$ Jacobian matrix and that of $\boldsymbol{J}_c$ is a $(6 \times (6-f))$ constraint matrix, where f is the total DoF. Note that the extended joint velocity, $\dot{\boldsymbol{q}}_e = [\dot{\boldsymbol{q}}^T; \boldsymbol{0}^T]^T$ is composed of usual joint velocity $\dot{\boldsymbol{q}}$ and zero for constraints, $\boldsymbol{J}_c$.

The inverse rate kinematics of Eq. (17) can be obtained by inverting $\boldsymbol{J}_e$ in Eq. (17):

$$\dot{\boldsymbol{q}}_e = \boldsymbol{J}_e^{-1} \dot{\boldsymbol{x}} = \boldsymbol{G}_e^T \dot{\boldsymbol{x}} = \begin{bmatrix} \boldsymbol{G}_j^T \\ \boldsymbol{G}_c^T \end{bmatrix} \dot{\boldsymbol{x}} \tag{18}$$

where $\boldsymbol{G}_e^T$ is the inverse of $\boldsymbol{J}_e$, and the two have the following mutually inverse relation as:

$$\boldsymbol{J}_e \boldsymbol{G}_e^T = \boldsymbol{G}_e^T \boldsymbol{J}_e \tag{19}$$

$$\boldsymbol{J}_j \boldsymbol{G}_j^T + \boldsymbol{J}_c \boldsymbol{G}_c^T = \boldsymbol{I}_6 \tag{20}$$

$$\begin{aligned} \boldsymbol{G}_j^T \boldsymbol{J}_j &= \boldsymbol{I}_f \\ \boldsymbol{G}_c^T \boldsymbol{J}_c &= \boldsymbol{I}_{(6-f)} \end{aligned} \tag{21}$$

$$\begin{aligned} \boldsymbol{G}_c^T \boldsymbol{J}_j &= \boldsymbol{0}_{(6-f)\times f} \\ \boldsymbol{G}_j^T \boldsymbol{J}_c &= \boldsymbol{0}_{f\times(6-f)}. \end{aligned} \tag{22}$$

The result has shown that the first term, $\boldsymbol{J}_e\boldsymbol{G}_e^T$, of Eq. (19) gives Eq. (20) whereas the second term, $\boldsymbol{G}_e^T\boldsymbol{J}_e$, gives Eqs. (21) and (22) with its sub-matrices.

If we can find $\boldsymbol{J}_c$ that satisfies Eqs. (21) and (22), constraints can be included in the rate kinematics as in Eqs. (17) and (18). Matrix $\boldsymbol{J}_c$ is a $6 \times (6-f)$ dimension that spans the orthogonal complementary subspace of $\boldsymbol{J}_j$. The range space of $\boldsymbol{J}_c$ represents the null-space of $\boldsymbol{J}_j^T$ and from the physical phenomenon perspective it represents the space that the manipulator cannot reach. If the columns of $\boldsymbol{J}_j$ are considered as a screw system, then the columns of $\boldsymbol{J}_c$ can be obtained from the reciprocal screw system of $\boldsymbol{J}_j$. A reciprocity relation is a well-known approach, and there are geometric, numeric, and analytic techniques to obtain the reciprocal screw's basis element. Geometric and numeric approaches suffer from two contradicting limitations. On the one hand, the geometric method is well-related to the physical meaning, but it cannot be consistently applied to complicated systems. On the other hand, the numerical method cannot be easily interpreted, but it can solve any screw system. This study uses an analytic approach introduced by Kim and Chung [20], since it can give a consistent derivation process with physical and geometrical meanings.

For PMs, the IMS is the intersection of all limb's IMS and the IRS is the union of the IRS for all limbs.

$$\text{IMS} = \cap_{i=1}^{n_l}\text{IMS}_i = \cap_{i=1}^{n_l}\mathcal{C}(\boldsymbol{J}_{ji}) \tag{23}$$

$$\text{IRS} = (\cap_{i=1}^{n_l}\text{IMS}_i)^c = \cup_{i=1}^{n_l}\mathcal{C}(\boldsymbol{J}_{ci}) \tag{24}$$

where $[\cdot]^c$ is a complementary subspace.

The basics of the screw presentation are given in Appendix A. Based on the screw operator called reciprocity, the IRS of a manipulator can be analytically obtained as follows from the given screw system:

$$\begin{bmatrix}\boldsymbol{M}_{i\parallel} & \boldsymbol{M}_{i\perp}\end{bmatrix} \wedge \$_{ci} = \begin{bmatrix}\boldsymbol{M}_{i\parallel} & \boldsymbol{M}_{i\perp}\end{bmatrix}\begin{bmatrix}\boldsymbol{s}_{ci\perp} \\ \boldsymbol{s}_{ci\parallel}\end{bmatrix} = \boldsymbol{0} \tag{25}$$

where $\boldsymbol{M}_{i\parallel}$ and $\boldsymbol{M}_{i\perp}$ denotes the direction and the moment vectors of the screw system, respectively.

4.2. Analytic velocity-level constraint equation

As stated earlier, even though numerical and geometric methods are alternatives to embedding structural constraints at the velocity level, an analytic approach is used in this study to enable further analysis. A general process was used to obtain the constraint-embedded extended Jacobian in [20], and here a specific case shown in Fig. 1 will be considered. Each limb (from the center of the fixed plate to the spherical joint A_i) forms a five system ($4\$_0 - 1\$_\infty$) by modeling joints as five single DoF kinematic pairs, and then the usual Jacobian matrix that generates limbs' IMS is given as follows:

$$\boldsymbol{J}_i = \begin{bmatrix}\boldsymbol{0} & \boldsymbol{s}_{2i_\parallel} & \boldsymbol{s}_{3i_\parallel} & \boldsymbol{s}_{4i_\parallel} & \boldsymbol{s}_{5i_\parallel} \\ \boldsymbol{s}_{1i_\parallel} & \boldsymbol{s}_{2i_\parallel} \times \boldsymbol{l}_i & \boldsymbol{0} & \boldsymbol{0} & \boldsymbol{0}\end{bmatrix}. \tag{26}$$

A screw reciprocal to the screw system $\boldsymbol{J}_i$ in Eq. (26) has the following relations, as in Eq. (25):

$$\begin{bmatrix}\boldsymbol{M}_\parallel & \boldsymbol{M}_\perp\end{bmatrix}\$_{ci} = \begin{bmatrix}\boldsymbol{s}_{5i_\parallel}^T & \boldsymbol{0}^T \\ \boldsymbol{s}_{4i_\parallel}^T & \boldsymbol{0}^T \\ \boldsymbol{s}_{3i_\parallel}^T & \boldsymbol{0}^T \\ \boldsymbol{s}_{2i_\parallel}^T & (\boldsymbol{s}_{2i_\parallel} \times \boldsymbol{l}_i)^T \\ \boldsymbol{0}^T & s_{1i_\parallel}^T\end{bmatrix}\begin{bmatrix}\boldsymbol{s}_{ci_\perp} \\ \boldsymbol{s}_{ci_\parallel}\end{bmatrix} = \boldsymbol{0}. \tag{27}$$

Then, as given in [20], the direction vector of the reciprocal screw can be obtained from Eq. (27):

$$\begin{aligned}\boldsymbol{s}_{ci_\parallel} = &-[\boldsymbol{s}_{5i_\parallel} \cdot (\boldsymbol{s}_{3i_\parallel} \times \boldsymbol{s}_{2i_\parallel})]\left(\boldsymbol{r}_{54} \times \boldsymbol{s}_{4i_\parallel}\right) \times \boldsymbol{s}_{1i_\parallel} + [\boldsymbol{s}_{5i_\parallel} \cdot (\boldsymbol{s}_{4i_\parallel} \times \boldsymbol{s}_{2i_\parallel})]\left(\boldsymbol{r}_{53} \times \boldsymbol{s}_{3i_\parallel}\right) \times \boldsymbol{s}_{1i_\parallel} \\ &- [\boldsymbol{s}_{5i_\parallel} \cdot (\boldsymbol{s}_{4i_\parallel} \times \boldsymbol{s}_{3i_\parallel})]\left(\boldsymbol{r}_{52} \times \boldsymbol{s}_{2i_\parallel}\right) \times \boldsymbol{s}_{1i_\parallel}\end{aligned} \tag{28}$$

where $\boldsymbol{r}_{5i} = \boldsymbol{r}_i - \boldsymbol{r}_5$ is the relative moment arm between the fifth and ith joints. Because of the same spherical joint with zero moment arm, $\boldsymbol{r}_{54} = \boldsymbol{r}_{53} = \boldsymbol{0}$, and $\boldsymbol{r}_{52} = \boldsymbol{l}_i$. Equation (28) can be further simplified by the above moment arm relations and the vector triple product

$$\boldsymbol{s}_{ci_\parallel} = -[\boldsymbol{s}_{5i_\parallel} \cdot (\boldsymbol{s}_{4i_\parallel} \times \boldsymbol{s}_{3i_\parallel})]\left(\boldsymbol{l}_i \times \boldsymbol{s}_{2i_\parallel}\right) \times \boldsymbol{s}_{1i_\parallel} \tag{29}$$

$$\approx \left(\boldsymbol{l}_i \times \boldsymbol{s}_{2i_\parallel}\right) \times \boldsymbol{s}_{1i_\parallel} \quad \because \text{unit direction vector} \tag{30}$$

$$= (\boldsymbol{s}_{1i_\parallel} \cdot \boldsymbol{l}_i)\boldsymbol{s}_{2i_\parallel} - (\boldsymbol{s}_{1i_\parallel} \cdot \boldsymbol{s}_{2i_\parallel})\boldsymbol{l}_i \tag{31}$$

$$\approx s_{2i_\parallel} \qquad \because \boldsymbol{s}_{1i_\parallel} \perp \boldsymbol{s}_{2i_\parallel} \text{ and unit direction vector.} \tag{32}$$

With the direction vector in Eq. (32), the moment vector of the reciprocal screw can be obtained from Eq. (27), and yields the result of $\boldsymbol{s}_{ci_\perp} = \mathbf{0}$. Then,the final twist of non-freedom is a form of $\$_\infty$ screw:

$$\$_{ci} = \begin{bmatrix} \mathbf{0} & \boldsymbol{s}_{2i_\parallel} \end{bmatrix}^T. \tag{33}$$

By embedding the restriction twist into the limb Jacobian, we can obtain extended Jacobian :

$$\boldsymbol{J}_{ei} = \begin{bmatrix} \mathbf{0} & \boldsymbol{s}_{2i_\parallel} & \boldsymbol{s}_{3i_\parallel} & \boldsymbol{s}_{4i_\parallel} & \boldsymbol{s}_{5i_\parallel} & \mathbf{0} \\ \boldsymbol{s}_{1i_\parallel} & \boldsymbol{s}_{2i_\parallel} \times \boldsymbol{l}_i & \mathbf{0} & \mathbf{0} & \mathbf{0} & \boldsymbol{s}_{2i_\parallel} \end{bmatrix}. \tag{34}$$

Since the manipulator has three identical limbs, analyzing a single chain is sufficient to determine the entire manipulator constraint. For the limb, point A_i is regarded as the reference point of motion, but for the manipulator, the reference point of motion must be moved to the center of the moving platform by the following transformation matrix:

$$\boldsymbol{M} = \begin{bmatrix} \boldsymbol{I} & \mathbf{0} \\ -[\boldsymbol{a}_i\times] & \boldsymbol{I} \end{bmatrix} \tag{35}$$

where $\boldsymbol{a}_i$ is a radial vector from the center of the moving platform to point A_i based on the fixed frame.

Hence, by pre-multiplying Eq. (35) with $\boldsymbol{J}_{ei}$ of Eq. (34), the extended Jacobian of limb i can be obtained with the reference point on the moving platform. The inverse relation of the extend Jacobian of limb i can also be obtained similarly in Eqs. (28)–(33) for the active joint and constraints, which have been described in detail in [20,22].

The final form of the inverse-rate kinematics (IRK) of the entire manipulator can be described as follows:

$$\begin{bmatrix} \dot{\boldsymbol{q}}_a \\ \mathbf{0} \end{bmatrix} = \begin{bmatrix} \boldsymbol{G}_a^T \\ \boldsymbol{G}_c^T \end{bmatrix} \dot{\boldsymbol{x}} \tag{36}$$

where $\dot{\boldsymbol{q}}_a$ and $\dot{\boldsymbol{x}}$ denote the active joint velocity and moving platform velocity, respectively, and $\boldsymbol{G}_a^T$ and $\boldsymbol{G}_c^T$ denote the wrench system or inverse relation of the active joint and constraint, respectively.

In most cases, we only consider the active joint motion in the velocity relation without considering the constraints. However, with the extended Jacobian relation, we consider motion and constraints simultaneously to describe the kinematics, by which we can analyze the effect of the constraints on manipulator's motion.

For the 3-PRS manipulator, the constraint matrix in $\boldsymbol{G}_c^T$ has the following form:

$$\boldsymbol{G}_c^T = \begin{bmatrix} \boldsymbol{s}_{21_\parallel}^T & (\boldsymbol{s}_{21_\parallel} \times \boldsymbol{a}_1)^T \\ \boldsymbol{s}_{22_\parallel}^T & (\boldsymbol{s}_{22_\parallel} \times \boldsymbol{a}_2)^T \\ \boldsymbol{s}_{23_\parallel}^T & (\boldsymbol{s}_{23_\parallel} \times \boldsymbol{a}_3)^T \end{bmatrix}. \tag{37}$$

To operate the manipulator, the constraints in Eq. (37) must be satisfied to produce zero velocity for the given input motion.

5. Properties of constraint matrix

For PMs with less than 6-DoFs, constraints induced from each leg govern the manipulator's entire motion. In previous sections, we derived constraint relations based on geometric and analytic approaches at the position and velocity levels, respectively. In this section, we take the time derivative of position level point-plane constraint to show the algebraic equivalency between the two approaches.

Hence, it can be clear that using position constraint to obtain velocity parasitic motion is not mandatory for velocity based control scheme, and with the analytic constraint equation described by Eq. (37), further properties are analyzed eventually.

Comparison of position and velocity level constraint

This section presents an algebraic equivalency between the point-plane geometric position-level and the analytic velocity-level constraint. To demonstrate this, we take the time-derivative of the position level constraint given in Eq. (9). The procedure begins by expanding Eq. (9) to the following form:

$$\boldsymbol{p}^T \boldsymbol{s}_{2i\parallel} + \boldsymbol{R}\boldsymbol{a}_i'^T \boldsymbol{s}_{2i\parallel} = 0. \tag{38}$$

The differentiation of Eq. (38) with respect to time gives the following:

$$\dot{\boldsymbol{p}}^T \boldsymbol{s}_{2i\parallel} + \dot{\boldsymbol{R}}\boldsymbol{a}_i'^T \boldsymbol{s}_{2i\parallel} = 0 \tag{39}$$

$$\dot{\boldsymbol{p}}^T \boldsymbol{s}_{2i\parallel} + (\boldsymbol{\omega} \times (\boldsymbol{R}\boldsymbol{a}_i'))^T \boldsymbol{s}_{2i\parallel} = 0 \tag{40}$$

$$\boldsymbol{s}_{2i\|}^T \dot{\boldsymbol{p}} + (\boldsymbol{s}_{2i\|} \times \boldsymbol{a}_i)^T \boldsymbol{\omega} = 0 \tag{41}$$

$$\begin{bmatrix} \boldsymbol{s}_{2i\|}^T & (\boldsymbol{s}_{2i\|} \times \boldsymbol{a}_i)^T \end{bmatrix} \begin{bmatrix} \dot{\boldsymbol{p}} \\ \boldsymbol{\omega} \end{bmatrix} = 0. \tag{42}$$

By applying $i = 1, 2$, and 3 in Eq. (42) for three limbs, the constraint can be written as a matrix to represent the entire manipulator constraint and this matrix is equal to Eq. (37). As expected, the geometric structural constraint obtained in Eq. (42) by taking the time derivative of Eq. (9) and the analytic constraints Eq. (37) in Section 4.2 gives exactly the same algebraic expression. However, the analytic equation derived in Section 4 is more systematic, and the same process can be applied to other manipulators to obtain the constraint embedded-extended Jacobian and constraints. As a result, analysis and further study of the parasitic motion can be systematic and insightful.

5.1. Constraint-compatible task velocity

For the general case, we can assign an arbitrary desired motion for the manipulator to follow, but for a manipulator with less than 6-DoFs, we cannot assign an arbitrary desired motion because we cannot guarantee that the given desired motion will satisfy the structural constraints. If a given desired motion does not satisfy the constraints, then the manipulator will fail, which is the worst case scenario. For PMs, constraints are changed at every instant and they are simultaneously related to all legs. These complicated relations find the constraint-compatible desired motion more challenging.

As shown in Eq. (36), if a motion $\dot{\boldsymbol{x}}$ is constraint-compatible, the motion is mapped to the null-space with $\boldsymbol{0} = \boldsymbol{G}_c^T \dot{\boldsymbol{x}}$. Consequently, the constraint-compatible motion $\dot{\boldsymbol{x}}$ is in the null space of $\boldsymbol{G}_c^T$ and can be expressed as follows:

$$\dot{\boldsymbol{x}} = \left(\boldsymbol{I} - \boldsymbol{G}_c \boldsymbol{G}_c^{\dagger}\right) \dot{\boldsymbol{x}}_a \tag{43}$$

where $\dot{\boldsymbol{x}}_a \in \mathbb{R}^6$ denotes an arbitrary motion without considering constraints and $(\cdot)^{\dagger}$ is the MoorePenrose inverse. As $\dot{\boldsymbol{x}}_a$ varies, all feasible solution that is compatible with the structural constraint policy of the manipulator are generated is the physical interpretation of Eq. (43).

By using a constraint-compatible motion $\dot{\boldsymbol{x}}$, the inverse rate kinematics in Eq. (36) can be solved safely. However, the constraint-compatible motion $\dot{\boldsymbol{x}}$ is not equal to the given desired motion $\dot{\boldsymbol{x}}_a$, and thus, the manipulator cannot be controlled as we desired every time because of the constraints, which causes the parasitic motion. In this projection method the main independent motion and the parasitic motion are obtained simultaneously, however, sometimes we need to distinguish them.

5.2. A procedure to distinguish the parasitic terms from the independent terms

To the best of the authors' knowledge, no known method is introduced to systematically detect and distinguish the task variable parasitic term from the independent ones either at the position or velocity level. Considering this, we have presented a systematic procedure to detect the parasitic motion, identify their type and the corresponding direction in this subsection. It is important to note that the complete inverse rate kinematics (IRK) of the manipulator is required to apply the proposed procedure for identifying the parasitic motion.

The core idea of the presented procedure is originated from the definition of parasitic motion. As defined by several researchers and in this paper, parasitic motion accompanies the main (independent) motion and occurs following the independent user input tasks. Hence, they cannot generate joint motion on their own. By utilizing the interesting feature of Eq. (43), each term of $\dot{\boldsymbol{x}}_a$ can be filtered and consecutively applied to Eq. (36) to get the joint rate. Then, some terms of $\dot{\boldsymbol{x}}_a$ do not generate a motion to change the manipulator pose while others move it to the new desired configuration. The terms that do not modify the manipulator to the desired posture are the parasitic (dependent) task variables and the otherwise independent parameter representing the DoF of the manipulator.

Below is the step by step basis procedure that can be used to distinguish the parasitic (dependent) terms.

- First, the IMS and IRS of the manipulator are derived analytically based on the theory of screw.
- Then, give the desired task velocity trajectory ($\dot{\boldsymbol{x}}_a$) to Eq. (43) independently for each axis, and obtain the corresponding constraint-compatible motion.
- Next, the constraint-compatible velocity obtained from Eq. (43) of step two is applied to IRK to get the joint velocity.
- Check the result of IRK for each input task motion and simultaneously check $\dot{\boldsymbol{x}}$ of Eq. (43) to identify what changes have been made to its elements.
- If the selected input motion is the dependent (parasitic) term, there will be no joint motion. Because the parasitic motion is dependent, and it occurs only when independent variables are provided as an input. Otherwise, the selected input term is regarded as the independent one.
- Repeat the procedure for all six terms of the task-space variables and consider the terms that do not generate joint motion by themselves as the parasitic terms and the otherwise independent component.

- At this stage, we detected if the parasitic motion exists in the manipulator, and the type (direction) of the parasitic motion are also known simultaneously.

In summary, using Eq. (43) and IRK, we obtained the method to identify the dependent terms from the independent terms.

The result with the presented procedure clearly showed the parasitic (dependent) terms could not generate leg velocity alone. On the other hand, independent terms can generate a leg motion and the parasitic motion as well. So, our approach can distinguish these two terms without ambiguity following the above procedures.

5.3. Velocity level coupling relation

Although the approach presented in Section 5.1 can generate an appropriate parasitic motion that is required to satisfy the structural constraint, it is quite important to explicitly and analytically obtain the parasitic motion equation. One should know the reason that induces a parasitic motion if he/she needs to optimize it or design a novel manipulator without parasitic motion. To achieve this, an analytic coupling relation between the parasitic and independent term plays key role. In this section, by using the matrix form of the constraint equation represented by Eq. (37), the velocity level coupling is obtained, after which we can identify the parameters that contribute to parasitic motion. The coupling relation represents a parasitic motion as a function of independent motion. Usually, this problem is addressed at the position level [1,8,9] even when dealing with the velocity [4] and dynamics [25]. This section will derive the coupling relation directly from the analytic constraint matrix at the velocity level.

Variables v_z, ω_x, and ω_y were identified as independent variables in the previous sections, particularly in Section 5.2, whereas v_x, v_y, and ω_z were the parasitic and thus can be expressed as a function of the independent variables. Accordingly, the problem can be formulated as shown below:

$$\begin{bmatrix} v_x \\ v_y \\ \omega_z \end{bmatrix} = f\left(\begin{bmatrix} \omega_x \\ \omega_y \\ v_z \end{bmatrix}\right) \tag{44}$$

From the rate kinematics relation we have :

$$\boldsymbol{G}_c^T \dot{\boldsymbol{x}} = \boldsymbol{0} \tag{45}$$

Equation (45) can rewrite as below for the ith since all legs are identical.

$$\boldsymbol{s}_{2i_\parallel}^T \boldsymbol{v} + [\boldsymbol{s}_{2i_\parallel} \times] \boldsymbol{a}_i \boldsymbol{\omega} = 0 \tag{46}$$

where $[\boldsymbol{s}_{2i\parallel} \times]$ is the skew symmetric matrix. The elements of Eq. (46) can be reorganized by collecting the parasitic terms in one side and independent terms the other side as follows.

$$-v_x s\xi_i + v_y c\xi_i + \omega_x a_{iz} c\xi_i + \omega_y a_{iz} s\xi_i + \omega_z(-a_{ix} c\xi_i - a_{iy} s\xi_i) = 0. \tag{47}$$

Note that parasitic terms can be identified using the procedure suggested in Section 5.2 if the mechanism is not previously studied. Rearranging Eq. (47) and adding all the leg relations to obtain the form of Eq. (44) give the following relation:

$$\begin{bmatrix} v_x \\ v_y \\ \omega_z \end{bmatrix} = \boldsymbol{C}_1^{-1} \boldsymbol{C}_2 \begin{bmatrix} \omega_x \\ \omega_y \end{bmatrix} \tag{48}$$

where

$$\boldsymbol{C}_1 = \begin{bmatrix} -s_{\xi_1} & c_{\xi_1} & -(a_{1x}c_{\xi_1} + a_{1y}s_{\xi_1}) \\ -s_{\xi_2} & c_{\xi_2} & -(a_{2x}c_{\xi_2} + a_{2y}s_{\xi_2}) \\ -s_{\xi_3} & c_{\xi_3} & -(a_{3x}c_{\xi_3} + a_{3y}s_{\xi_3}) \end{bmatrix}, \quad \boldsymbol{C}_2 = \begin{bmatrix} -a_{1z}c_{\xi_1} & -a_{1z}s_{\xi_1} \\ -a_{2z}c_{\xi_2} & -a_{2z}s_{\xi_2} \\ -a_{3z}c_{\xi_3} & -a_{3z}s_{\xi_3} \end{bmatrix}. \tag{49}$$

The results obtained in this section can be utilized for many kinematics studies, including those dedicated to velocity-level optimization, which is in our future work plan, and obtaining the constraint-compatible motion. This is because v_x, v_y, and ω_z are solved in a way that satisfies the structural constraint. From Eq. (48), we can see that the linear velocity in the direction of the z-axis does not contribute to the generation of parasitic motion, but the orientation variables ω_x and ω_y generate parasitic motion. Additionally, Eq. (48) and Eq. (49) reveals the angle for leg positions ξ_i, and the radius of moving platform r_p are structural parameters that affects the parasitic motion. Accordingly, one can use this revealing information to eliminate parasitic motion or derive a new mechanism out of the existing ones.

6. Numerical validation

In this section, numerical simulation is presented to validate the proposed approach. The geometric parameters used for simulation shown in Table 1 are adopted from Carretero et al. [1].

To demonstrate the effect of structural constraint on the input motion, Fig. 3 is presented with a desired velocity:

$$\dot{\boldsymbol{x}}_a = \begin{bmatrix} 0 & 0 & 0 & 0.2s2\pi t & -0.2c2\pi t & 0 \end{bmatrix}^T.$$

Table 1
Geometric parameters.

Variable	Value	unit
Plate radius (r_p)	1000	mm
Leg length (l)	1000	mm
z position	707.1068	mm
ψ and θ	±0.2	rad

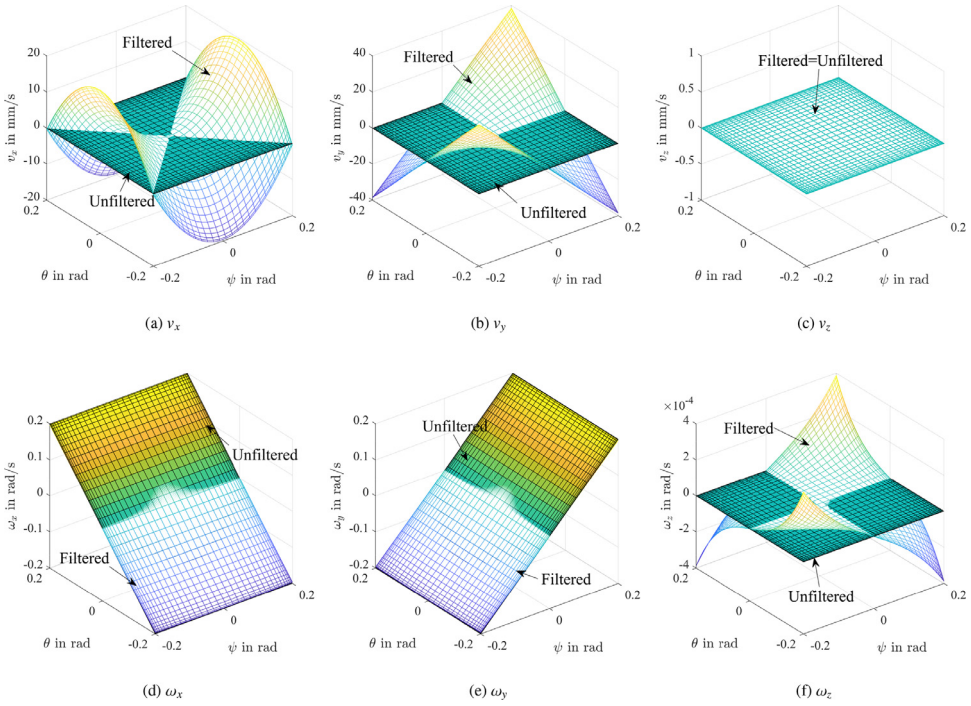

Fig. 3. The effect of structural constraint on the input velocity.

$\dot{\boldsymbol{x}}_a$ comprises a rotational motion about the x- and y-axes. Although $\dot{\boldsymbol{x}}_a$ is the task we want to execute, the manipulator requires further information to properly operate i.e. parasitic motion information. By providing $\dot{\boldsymbol{x}}_a$ to Eq. (43), ours and manipulators requirement are consolidated. From the simulation, it is evident that the filtering matrix Eq. (43) modifies the input velocity $\dot{\boldsymbol{x}}_a$ in the optimal sense, to make it compatible with its structural constraint. As we discussed earlier, our desired input and the task that the manipulator can execute must agree, and is done by Eq. (43) in this example of demonstrating the effect of structural constraint on the input velocity.

The simulation is provided for the entire workspace to give a clear image of what happens in the manipulator's complete configuration regardless of z-axis translation. For the parasitic motion, Fig. 3a and b shows the linear velocity in the x(y) direction, which is entirely different from a given input motion to the filter equation. Although zero motion is provided, the manipulator has forcefully generated some velocity profiles to comply with the internal structural constraint; i.e., the linear parasitic motion. Similarly, Fig. 3f shows the induced amplitude of the parasitic motion angular velocity about the z-axis. The filtering matrix modifies our input zero velocity, and a small rotational motion occurs to meet the structural requirement. Hence, the manipulator securely operates with these small auto-generated motions, which is undesirable.

Regarding the main motions, the z-axis translation is not affected by Eq. (43) as can be seen in Fig. 3c and Eq. (48). Moreover, the independent angular velocities (ω_x and ω_y) are not profoundly changed as of the parasitic terms by the projection matrix since inputs in these coordinates are the DoFs of the manipulator. Hence, the user desired motions is preserved while the undesired parasitic motions are automatically generated to satisfy the manipulator requirement.

According to Fig. 3d and e, Eq. (43) slightly adjusts the magnitude of ω_x and ω_y and is an optimal projection. This indicates, however, if our input in the main coordinates are too large and violate the constraint, the filtering matrix, Eq. (43), also modifies the magnitude of input motion in the main direction to ensure the manipulator operates in a safe range.

From the simulation, we can clearly see the abstract phenomenon of parallel manipulators with parasitic motion is well demonstrated with Eq. (43) and is required in to comply the desired motion with the structural constraint policy.

Note that the modified motion might be considerably inconvenient from the user's perspective depending on the application. Hence, the result obtained in Section 5.3 can be used for further analysis which is our future work. According to the

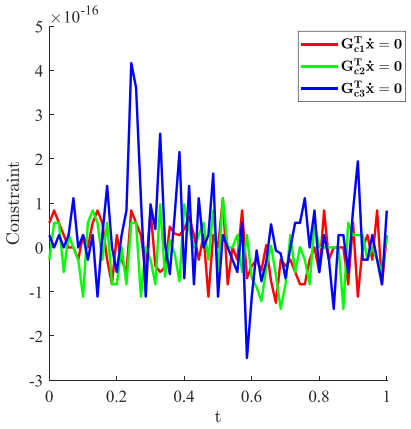

Fig. 4. Constraint condition test using Eq. (43).

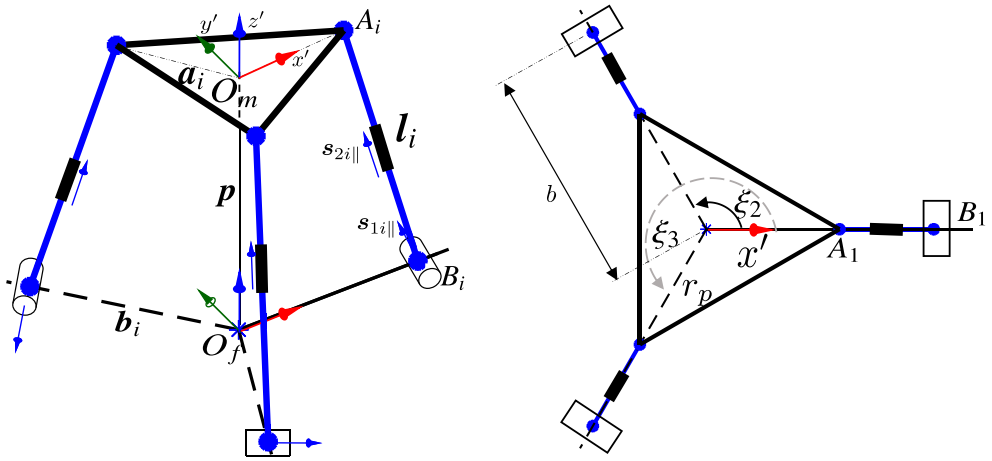

Fig. 5. 3-RPS manipulator schematics.

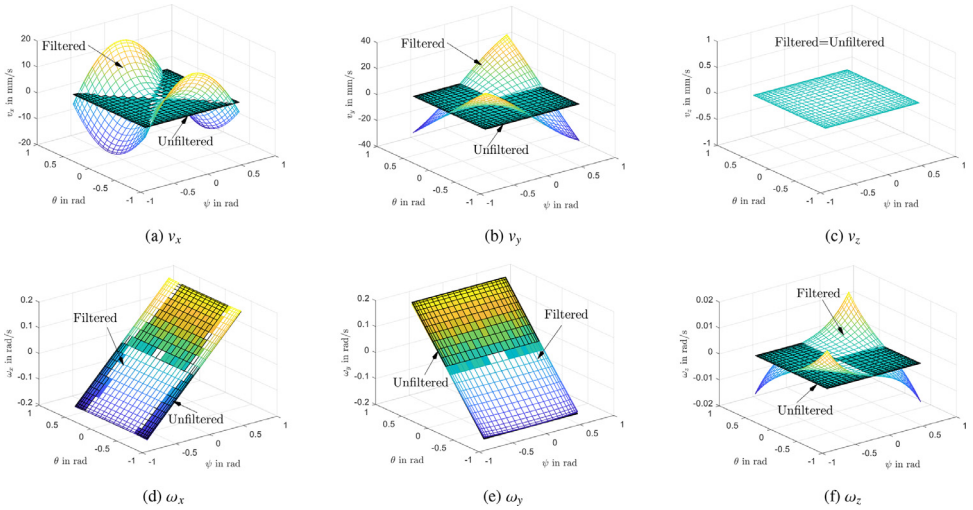

Fig. 6. The effect of 3-RPS structural constraint on the input velocity.

result presented in this paper, any arbitrary desired velocity provided to Eq. (43) gives a constraint-compatible motion that satisfies the constraint in Eq. (36), as shown in Fig. 4. Therefore, the solution lies always in the range space of $\boldsymbol{G}_j$ and is the basis element of instantaneous motion space (IMS).

To demonstrate the approach with different example, a numerical simulation of the 3-RPS manipulator shown in Fig. 5 is included. The manipulator constraint equation is derived by the method shown in Section 4 as:

$$\boldsymbol{G}_c^T = \begin{bmatrix} \boldsymbol{s}_{11\|}^T & (\boldsymbol{s}_{11\|} \times \boldsymbol{a}_1)^T \\ \boldsymbol{s}_{12\|}^T & (\boldsymbol{s}_{12\|} \times \boldsymbol{a}_2)^T \\ \boldsymbol{s}_{13\|}^T & (\boldsymbol{s}_{13\|} \times \boldsymbol{a}_3)^T \end{bmatrix} \tag{50}$$

The numerical simulation is performed using the same user-desired motion utilized for the 3-PRS manipulator. The simulation shown in Fig. 6 demonstrates the parasitic motion induced to satisfy the constraints in response to the independent user-desired input motion. These parasitic motions are v_x, v_y, and ω_z shown in Fig. 6a, b, and f, respectively. With the task-velocity obtained in Fig. 6, the inverse rate kinematics can be accurately solved.

7. Conclusions

This study presented an approach to obtain the parasitic motion governing equation from the velocity level structural constraint condition. The study presented the position level method of describing parasitic motion for comparison with the proposed approach. Although the result indicates that the analytical and geometric constraints can equivalently incorporate the constraint information and get the parasitic motion equation, the analytic constraint is better for consistency and further analysis of the constraint. Moreover, by utilizing the analytic constraint matrix property, a constraint-compatible desired task velocity can be obtained and safely applied to the manipulator without considering structural breakage due to the incorrect input assignment. The paper also introduced a systematic procedure to distinguish the task-space's main motion, and an explicit velocity level coupling relation is obtained directly from the analytic constraint relation. Besides, the constraint matrix effect on the input velocity is demonstrated in relation to the configuration change. To visualize the constraint matrix effect on the input motion, a velocity without parasitic motion is assigned to Eq. (43) and evaluated over the entire rotational workspace. The results confirm that the structure modifies the input motions and ensures that the velocity is compatible with the manipulator's internal structural constraint without altering the desired main motion.

Although the approach is evaluated utilizing the particular 3-PRS and 3-RPS manipulators, other manipulators parasitic motion can be detected using the proposed procedure and, analyzed by manipulating the elements of the velocity-level constraint matrix.

Declaration of Competing Interest

The authors declare that they have no known competing financial interest or personal relationship that could have appeared to influence the work reported in this paper.

Acknowledgment

This work was supported by the Korea Institute of Science and Technology (KIST) Institutional Program (2E30280).

Appendix A. The screw representation of finite motion

Based on Plücker's work in geometry, a line $\mathscr{L}(\boldsymbol{A}-\boldsymbol{B})$ in space depicted in Fig. A.7 can be described with six coordinates where three coordinates represent the direction ($\boldsymbol{s}_{\|} \in \mathbb{R}^3$) and the remaining three (($\boldsymbol{s}_{\|} \times \boldsymbol{p}$) $\in \mathbb{R}^3$) represents the moment

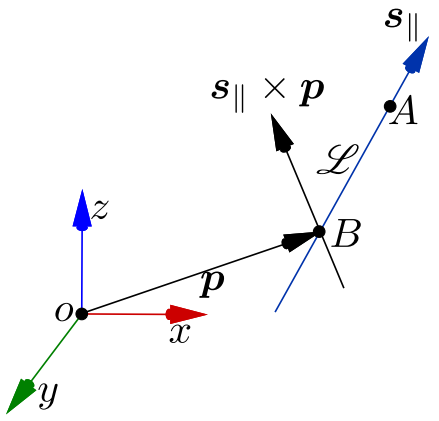

Fig. A.7. Screw representation.

as in Eq. (A.1). This line modeling concept acts as a basis for the description of rigid body motion and it extends to the kinematics via the screw theory.

Considering the physical screw(nut-bolt) that simultaneously undergoes rotation and translation movement, the kinematics can be represented by Plücker's line equation. Moreover, **Mozz-Chasles'** theorem states that any rigid body motion, can be represented by a spatial six-dimensional vector called screw ($\$ \in \mathbb{R}^6$). Therefore, the screw displacement consists of a rotation about the screw axis and a translation along the same axis, which can be represented by physical nut-bolt motion and is analogous to Plücker's line representation. Thus, the rigid body kinematics can also be represented by $\mathscr{L}(\boldsymbol{A}-\boldsymbol{B})$ as follows:

$$\$ = \begin{bmatrix} \boldsymbol{s}_{\parallel}^T & (\boldsymbol{s}_{\parallel} \times \boldsymbol{p})^T \end{bmatrix}^T. \tag{A.1}$$

A screw can be represented in the ray order if the direction vector is the first term $\begin{bmatrix} \boldsymbol{s}_{\parallel}^T & \boldsymbol{s}_{\perp}^T \end{bmatrix}^T$ or in the axis order if the moment vector is the first term $\begin{bmatrix} \boldsymbol{s}_{\perp}^T & \boldsymbol{s}_{\parallel}^T \end{bmatrix}^T$. Moreover, a screw can be an infinite pitch ($\$_\infty$) if the direction vector is negligibly zero because of infinite pitch; it can be zero pitch ($\$_0$) if the pitch is zero. These two screws are related to the two most common physical kinematic pairs, revolute and prismatic pairs; both of which are used in the design and manufacturing of robots. The zero pitch screw represents a revolute joint, whereas the infinite pitch screw represents a prismatic pair. A general, zero, and infinite screws can be mathematically represented as follows in the Plücker's ray order, respectively.

$$\$ = \begin{bmatrix} \boldsymbol{s}_{\parallel} \\ \boldsymbol{s}_{\parallel} \times \boldsymbol{p} + h\boldsymbol{s}_{\parallel} \end{bmatrix} \tag{A.2}$$

$$\$_0 = \begin{bmatrix} \boldsymbol{s}_{\parallel} \\ \boldsymbol{s}_{\parallel} \times \boldsymbol{p} \end{bmatrix} \tag{A.3}$$

$$\$_\infty = \begin{bmatrix} \boldsymbol{0} \\ \boldsymbol{s}_{\parallel} \end{bmatrix}. \tag{A.4}$$

In this paper, **Assumption 1** holds given that the actual common practice to generate motion between connected rigid bodies is based on the revolute and prismatic pairs.

Assumption 1: All kinematic chains in a manipulator are made from revolute, prismatic, or a combination of the two. Hence, the kinematic pairs in this paper can be represented by $\$_0$ or $\$_\infty$ screws, and the screw algebraic relations are derived based on this assumption.

For screws, $\$_1$ and $\$_2$ are given as follows:

$$\$_1 = \begin{bmatrix} \boldsymbol{s}_{1\parallel} \\ \boldsymbol{s}_{1\parallel} \times \boldsymbol{p_1} \end{bmatrix}, \quad \$_2 = \begin{bmatrix} \boldsymbol{s}_{2\parallel} \\ \boldsymbol{s}_{2\parallel} \times \boldsymbol{p_2} \end{bmatrix}$$

the most crucial algebraic operation known as reciprocal screw, can be described as:

$$\$_1 \wedge \$_2 = \boldsymbol{s}_{1\parallel}^T(\boldsymbol{s}_{2\parallel} \times \boldsymbol{p_2}) + (\boldsymbol{s}_{1\parallel} \times \boldsymbol{p_1})^T \boldsymbol{s}_{2\parallel} = 0 \tag{A.5}$$

where $\wedge = \begin{bmatrix} \boldsymbol{0} & \boldsymbol{I} \\ \boldsymbol{I} & \boldsymbol{0} \end{bmatrix}$ is the elliptic polar operator, which is used to interchange the order of direction and moment vectors of $\$_1$ and $\$_2$ switching from ray to axis and vice-versa [26]. Similarly, $\boldsymbol{I}$ represents a 3×3 unit matrix.

Supplementary materials

Supplementary material associated with this article can be found, in the online version, at doi:10.1016/j.mechmachtheory.2021.104409.

References

[1] J.A. Carretero, R.P. Podhorodeski, M.A. Nahon, C.M. Gosselin, Kinematic analysis and optimization of a new three degree-of-freedom spatial parallel manipulator, J. Mech. Des. Trans.ASME 122 (1) (2000) 17–24, doi:10.1115/1.533542.
[2] J.A. Carretero, M.A. Nahon, R.P. Podhorodeski, Workspace analysis and optimization of a novel 3-DOF parallel manipulator, Int. J. Rob. Autom. 15 (4) (2000) 178–188.
[3] Y.G. Li, H.T. Liu, X.M. Zhao, T. Huang, D.G. Chetwynd, Design of a 3-DOF PKM module for large structural component machining, Mech. Mach. Theory (2010), doi:10.1016/j.mechmachtheory.2010.01.008.
[4] Y. Liu, L. Wang, J. Wu, J. Wang, A comprehensive analysis of a 3-P (Pa) S spatial parallel manipulator, Front. Mech. Eng. 10 (1) (2015) 7–19, doi:10.1007/s11465-015-0324-3.
[5] A. Ruiz, F.J. Campa, C. Roldán-Paraponiaris, O. Altuzarra, C. Pinto, Experimental validation of the kinematic design of 3-PRS compliant parallel mechanisms, Mechatronics 39 (2016) 77–88, doi:10.1016/j.mechatronics.2016.08.006.
[6] Q. Li, Z. Chen, Q. Chen, C. Wu, X. Hu, Parasitic motion comparison of 3-PRS parallel mechanism with different limb arrangements, Robot. Comput. Integr. Manuf. 27 (2) (2011) 389–396, doi:10.1016/j.rcim.2010.08.007.

[7] J.A. Carretero, M. Nahon, C.M. Gosselin, B. Buckham, Kinematic analysis of a three-DOF parallel mechanism for telescope applications, in: Proceedings of the 1997 ASME Design Engineering Technical Conferences, Sacramento, California, 1997, pp. 1427–1435.
[8] X. Huo, T. Sun, Y. Song, A geometric algebra approach to determine motion/constraint, mobility and singularity of parallel mechanism, Mech. Mach. Theory 116 (2017) 273–293, doi:10.1016/j.mechmachtheory.2017.06.005.
[9] Y. Li, Q. Xu, Kinematic analysis of a 3-PRS parallel manipulator, Robot. Comput. Integr. Manuf. 23 (4) (2007) 395–408, doi:10.1016/j.rcim.2006.04.007.
[10] D. Gan, J.S. Dai, J. Dias, L. Seneviratne, Constraint-plane-based synthesis and topology variation of a class of metamorphic parallel mechanisms, J. Mech. Sci. Technol. 28 (10) (2014) 4179–4191, doi:10.1007/s12206-014-0931-7.
[11] Qinchuan Li, J.M. Hervé, 1T2R parallel mechanisms without parasitic motion, IEEE Trans. Rob. 26 (3) (2010) 401–410, doi:10.1109/TRO.2010.2047528.
[12] R. Lin, W. Guo, F. Gao, On parasitic motion of parallel mechanisms, in: Proceedings of the ASME Design Engineering Technical Conference, 2016, doi:10.1115/DETC2016-59859.
[13] L. Tsai, Robot analysis: the mechanics of serial and parallel manipulators, 1999.
[14] S.A. Joshi, L.W. Tsai, Jacobian analysis of limited-DOF parallel manipulators, J. Mech. Des. Trans.ASME 124 (2) (2002) 254–258, doi:10.1115/1.1469549.
[15] T. Huang, H.T. Liu, D.G. Chetwynd, Generalized Jacobian analysis of lower mobility manipulators, Mech. Mach. Theory 46 (6) (2011) 831–844, doi:10.1016/j.mechmachtheory.2011.01.009.
[16] T. Huang, S. Yang, M. Wang, T. Sun, D.G. Chetwynd, An approach to determining the unknown twist/wrench subspaces of lower mobility serial kinematic chains, J. Mech. Robot. 7 (3) (2015) 1–9, doi:10.1115/1.4028622.
[17] J. Zhao, B. Li, X. Yang, H. Yu, Geometrical method to determine the reciprocal screws and applications to parallel manipulators, Robotica 27 (6) (2009) 929–940, doi:10.1017/S0263574709005359.
[18] X. Kong, C. Gosselin, Virtual-chain approach for the type synthesis of parallel mechanisms, vol. 33, 2007. 10.1007/978-3-540-71990-8_5
[19] J.S. Dai, J.R. Jones, Null space construction using cofactors from a screw-algebra context, Proc. R. Soc. London Ser.A 458 (2024) (2002) 1845–1866, doi:10.1098/rspa.2001.0949.
[20] D. Kim, W.K. Chung, Analytic formulation of reciprocal screws and its application to nonredundant robot manipulators, J. Mech. Des. 125 (1) (2003) 158–164, doi:10.1115/1.1539508.
[21] J.S. Dai, J.R. Jones, A linear algebraic procedure in obtaining reciprocal screw systems, J. Robot. Syst. 20 (7) (2003) 401–412, doi:10.1002/rob.10094.
[22] D. Kim, Kinematic analysis of spatial parallel manipulators: analytic approach with the restriction space, Ph.D. thesis. Pohang University of Science and Technology, 2002.
[23] D. Kim, W. Chung, Y. Youm, Analytic Jacobian of in-parallel manipulators, in: Proceedings-IEEE International Conference on Robotics and Automation, 3, 2000, pp. 2376–2381, doi:10.1109/ROBOT.2000.846382.
[24] Y. Zhao, Y. Jin, J. Zhang, Kinetostatic modeling and analysis of an Exechon parallel kinematic machine(PKM) module, Chin. J. Mech. Eng. 29 (1) (2016) 33–44, doi:10.3901/CJME.2015.1012.120.
[25] M. Díaz-Rodríguez, J.A. Carretero, R. Bautista-Quintero, Solving the dynamic equations of a 3-PRS parallel manipulator for efficient model-based designs, Mech. Sci. 7 (1) (2016) 9–17, doi:10.5194/ms-7-9-2016.
[26] H. Lipkin, J. Duffy, The elliptic polarity of screws, J. Mech. Trans. Autom. Des. 107 (3) (1985) 377–386, doi:10.1115/1.3260725.